# MECHANICAL PERFORMANCE OF HIGH-ALTITUDE TILT-ROTOR BASED VTOL VEHICLE BASED ON FULL FLUID-STRUCTURE COUPLING METHOD

Xiayang Zhang, Qijun Zhao, Bo Wang, Guoqing Zhao

zhangxiayang@nuaa.edu.cn, qijunzhao@nuaa.edu.cn, wangbo@nuaa.edu.cn, zgq198495@nuaa.edu.cn

National Key Laboratory of Rotorcraft Aeromechanics, Nanjing University of Aeronautics and Astronautics, Nanjing, Jiangsu, China.

**Abstract**
Affected by the distinct structural characteristics, flight and operation conditions, the tilt-rotor system on an airship may endure aeroelastic instability under certain circumstances during actual envelope flight. Two typical configurations, i.e., beam-rotor layout and wing-rotor layout, are considered in this paper, and each physical model of the tilt-rotor system is established by means of fully fluid-structure coupling method. Because of the low-speed flight condition, the strip aerodynamic theory and the linear structural dynamic model are utilized for modelling. The aeroelastic characteristics of the tilt-rotor system are analyzed, in which the effects of rotation speed and distinct parameters on the aeroelastic characteristics of the models are discussed. The occurrence and evolution mechanism of the aeroelastic instability are revealed, which also provides guidance for the overall parameter design of the system.
Key words: tilt-rotor, aeroelasticity, instability, fluid-structure coupling

## 1. INTRODUCTION

Compared with conventional aircraft, the biggest advantage of airship is that it has unparalleled hovering time and can maintain flight ability in stratospheric altitude getting ride of atrocious weather. E.g., the flight time of traditional airplane is evaluated in hours, while the airship is measured in days or months. As shown in Fig. 1, the Airship also has great advantages in the task of detection, it can stay over the target for a long time to achieve persistent and accurate monitoring, e.g., the photoelectric radar system can clearly detect small ground targets in the travel of low-speed flight. Therefore, airship, as a kind of ultra-low speed or static large-scale aerial platform, has a wide application prospect in space development, communication relay, traffic monitoring, geological exploration, air transportation and other fields[1].

Fig. 1 The applications of airships in civilian and military fields

Airships are classified into low-speed aircraft because of their high inertia and low dynamic characteristics. It has the problem of underactuated control when it performs take-off and landing, dwelling, wind-resistant flight and trajectory tracking tasks[2]. On the one hand, the aerodynamic rudder surface installed on the hull has the problems of low structural stiffness, low efficiency and easy to be covered by the capsule body. On the other hand, conventional airships are only equipped with power devices with forward thrust, such as fixed propeller; the relevant pitch control needs to be adjusted by means of self-weight adjustment equipment and slider control; yaw control is adjusted by differential thrust of symmetrical propeller; controllable power and control tasks under complex conditions increase the demand of advanced power technique[3]. The actual flight test also proves that the controllability of the airship is under passive driving state when the airship flies against the wind. The application of vector propulsion technology can greatly improve the flight performance and control quality of the whole boat at the expense of less structural weight. In 2015, a medium-sized airship equipped with tail vector power device was successfully tested in Xilinguole, Inner Mongolia[4], proving that the controllability of the system has been greatly improved.

Compared with the conventional aircraft, the investigation of vector technology on airship started



Presented at 46th European Rotorcraft Forum, Moscow, Russia, 8-11 September, 2020

late. In fact, the airship has only been put into practice for nearly 20 years, and the development level is still in the stage of technical demonstration. Compared with the traditional vectoring-thrust device, airship vector power device has different operation conditions, which will affect the basic dynamic characteristics of the whole system further. Firstly, the body of airship is a flexible structure, which makes the root boundary conditions of vector system more flexible; at the meanwhile, it increases the structural requirements for lightweight and high strength. Secondly, the colossal capsule of airship makes it present low-dynamic and high-resistance structural and aerodynamic characteristics, so the real-time transient trim requirements need not be satisfied in the flight control design. Compared with the aerodynamic forces of the whole airship, the unsteady aerodynamic forces and moments caused by the rotation and tilting of the tilt rotor are negligible. Therefore, the dependence of the rotor on the periodic hinge, of the blade is relatively small. The rotor of airship vector power device is closer to the rigid propeller, and the stiffness of rotor brings more significant structural gyroscopic effect and increases the coupling effect between structural dimensions. These factors form the inherent characteristics of airship vector power device. Thirdly, the atmospheric environment during the envelope flight of airship is significantly different from that of conventional aircraft. A stratospheric airship will experience a 0-20 km altitude span when it performs takeoff mission flight. During this period, the change of atmospheric density will affect the aerodynamic characteristics of the wing and rotor, and then affect the aeroelastic dynamic characteristics of the whole vector device[5]. Under certain conditions, the whole system may even lose its stability. Thus, it is of great significance to carry out relevant academic research aimed to improving the safety design of the airship.

## 2. NOMENCLATURES

[B]: bifurcation

[D]: divergence

[F]: flutter

Raero: the aerodynamic factor of rotor
Waero: the aerodynamic factor of wing

## 3. MODELING

As shown in Fig.2, two typical configurations are considered for modeling. One is the beam-rotor case (BR-model), in which the rotor system is mounted on the supporting structure. The other is the wing-rotor case (WR-model), in which the addition of wing system can provide extra lift and controllable aerodynamic forces.

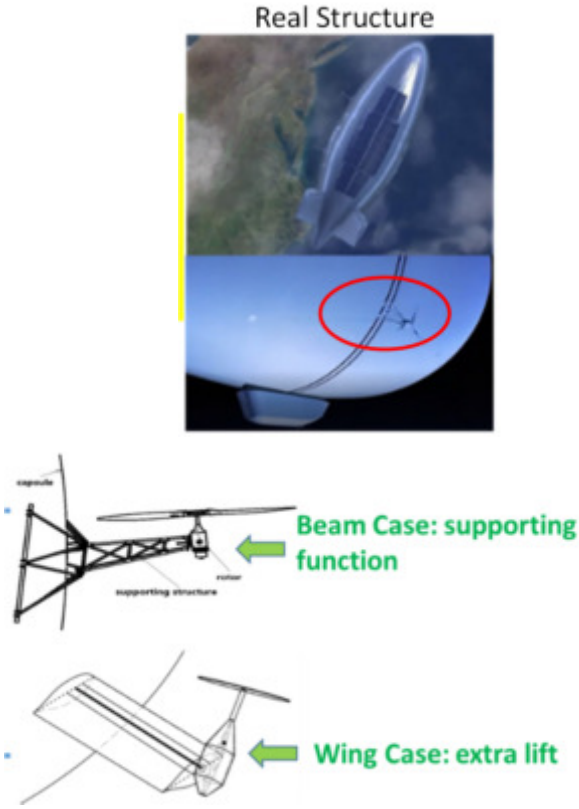


Fig. 2 Two general models of advanced high-altitude tilt-rotor based vehicle

Fig. 3 is a schematic overall view of the wing-rotor system. Wherein, the wing is fixed to the fuselage, whose span is $L_0$ and semi-chord is $b$; there is an offset $y_c$ between the center of mass of the wing and the elastic axis; the inertial coordinate system $ox_wy_wz_w$ is placed at the root elastic axis, the o point is the end point of the elastic axis, the $x_w$ axis is outside the elastic axis, the $y_w$ axis is arranged along the chord, and the $z_w$ axis follows the right hand screw rule. The tip rotor is fixed to the elastic axis of the wing, the center of gravity of the rotor is $G_t$ with a total mass of $m_t$ and an offset $r_0$; $Px_ry_rz_r$ is the root follower coordinate system, and the angular velocity of the rotor is $\Omega$.



Presented at 46th European Rotorcraft Forum, Moscow, Russia, 8-11 September, 2020

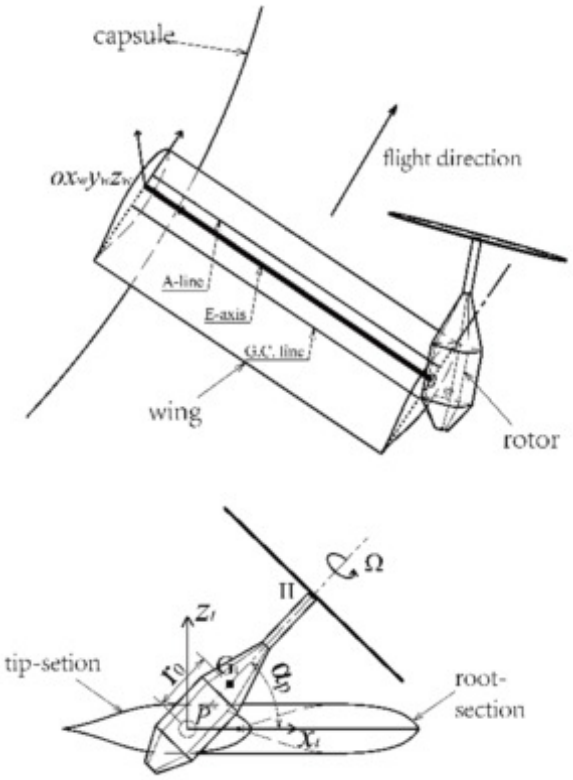


Fig. 3 Geometric parameters of the tilt-rotor system

### 3.1. Structural model

Hamilton's principle and Yamanaka's space equation considering the tip gyro-effect are introduced. According to the physical model established[6], the dynamic equation of the system can be expressed as

$$(1)\quad \begin{aligned} &-EI_y w^{(4)} - m_w \ddot{w} - m_w y_c \ddot{\theta} = 0 \\ &-EI_z v^{(4)} - m_w \ddot{v} = 0 \\ &GJ\theta'' - m_w y_c \ddot{w} - m_w r^2 \ddot{\theta} = 0 \end{aligned}$$

Where $EI_y$ and $EI_z$ are the elastic coefficients of the $y_w$ and $z_w$ directions of the elastic axis, respectively, $GJ$ is the torsional elastic coefficient of the elastic axis; $m_w$ is the linear density of the wing; $r$ is the equivalent radius of the inertia of the wing section; $w$, $v$, and $\theta$ are the displacement of the elastic axis in the $z_w$, $y_w$ direction and the torsion in the $x_w$ direction. $M_w$ and $L_w$ are the moment and lift force of the aerodynamic force per unit length along the pneumatic axis; the elastic axis adopts the formulized Euler-Bernoulli beam model.

The boundary conditions of the system at the end $x_w=L_0$ can be expressed as

(2)

$$\begin{aligned} &EI_y w^{(3)} - m_t \left( \ddot{w} + y_t \ddot{\theta} \right) = 0 \\ &EI_y w'' + J_y \ddot{w} + m_t z_t \left( z_t \ddot{w} - y_t \ddot{v} \right) = 0 \\ &EI_z v^{(3)} - m_t \left( \ddot{v} + z_t \ddot{\theta} \right) = 0 \\ &EI_z v'' + J_z \ddot{v} + m_t y_t \left( y_t \ddot{v} - z_t \ddot{w} \right) + J_y \Omega \dot{\theta} = 0 \\ &GJ\theta' + m_t z_t \left( \ddot{v} + z_t \ddot{\theta} \right) + m_t y_t \left( \ddot{w} + y_t \ddot{\theta} \right) + J_x \ddot{\theta} - J_y \Omega \dot{v} = 0 \end{aligned}$$

Wherein, $J_x$, $J_y$ and $J_z$ are the principal inertia of the rotor along $x_r$, $y_r$ and $z_r$ at the center of mass $G_t$. Rotor dynamics modeling takes into account the implicated motion at the end of the elastic axis, which specifically includes translational and rotational effects[6]. The system is flexible at the root $x_w=0$:

$$(3)\quad \begin{aligned} &EI_y w'' - k_4 w' = EI_z v'' - k_3 v' = EI_y w^{(3)} - k_2 w \\ &= EI_z v^{(3)} - k_1 v = GJ\theta' - k_5 \theta = 0 \end{aligned}$$

### 3.2. Aerodynamic model

The aerodynamic model based on strip theory shows the explicit variations expression of the aerodynamic forces, enabling the achievement of full coupling fluid-structure modelling.

#### 3.2.1. Wing aerodynamic model

The unsteady aerodynamic model is adopted to realize the modeling in frequency domain[7]. The aerodynamic force of the wing can be formulated as follows

$$L_w = \pi\rho_a b^2 \left[ -\ddot{w} + v_a \dot{\theta} - ba\ddot{\theta} \right] + 2\pi\rho_a v_a b C(k) \left[ v_a \theta - \dot{w} + b\left(\frac{1}{2} - a\right)\dot{\theta} \right]$$

$$(4)\quad \begin{aligned} M_w = {} & \pi\rho_a b^2 \left[ -ba\ddot{w} - v_a b\left(\frac{1}{2} - a\right)\dot{\theta} - b^2\left(\frac{1}{8} + a^2\right)\ddot{\theta} \right] \\ & + 2\pi\rho_a v_a b^2 \left(a + \frac{1}{2}\right) C(k) \left[ v_a \theta - \dot{w} + b\left(\frac{1}{2} - a\right)\dot{\theta} \right] \end{aligned}$$

Here, $a$ is the ratio of the distance between the elastic axis and the length of the semi chord, $\rho_a$ is the incoming flow density, $v_a$ is the velocity of the incoming flow, $k=\xi b/v_a$, $\xi$ is the angular frequency of vibration, and $C(k)$ is a known function of $k$.

#### 3.2.2. Rotor aerodynamic model

On the basis of the classic Johnson model[8], a variation model of aerodynamic force is developed to consider arbitrary tilt state.



Presented at 46th European Rotorcraft Forum, Moscow, Russia, 8-11 September, 2020

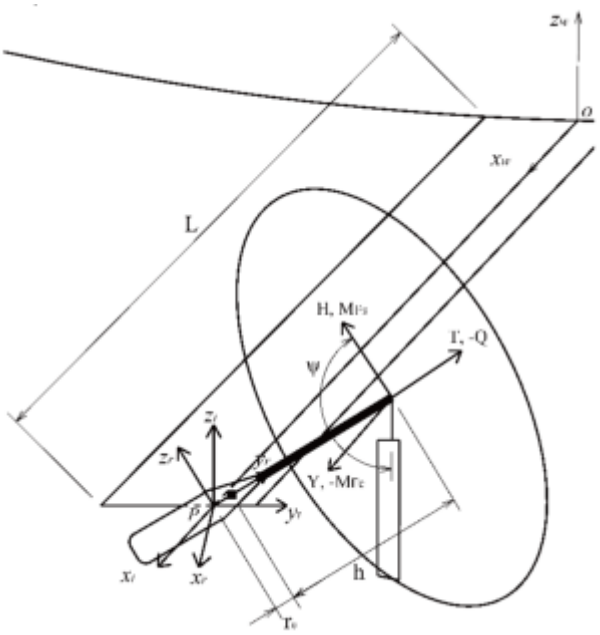


Fig. 4 The schemetic of rotor system

As shown in Fig. 4, the change of inflow conditions cause the change of aerodynamic force of each blade, thus changing the resultant force of air on the rotor disc. For a single blade, the variation of blade aerodynamic force can be expressed as

$$\delta\begin{bmatrix}F_p\\M_p\end{bmatrix}=\delta\left[Y,T,H,-M_{F_c}+Hh,-Q,M_{F_s}-Yh\right]^T \tag{5}$$

The vector $q_P=[x_p,y_p,z_p,a_x,a_y,a_z]^T$ at wing's tip E-axis point is introduced and the result of variation is transformed into the vector form within $Hx_ty_tz_t$ coordinate. Further, Eq.(5) is converted to overall $ox_wy_wz_w$ coordinate system.

$$\delta\begin{bmatrix}F_{tip}\\M_{tip}\end{bmatrix}=T_{wr}\delta\begin{bmatrix}F_p\\M_p\end{bmatrix}=\delta\left[F_{x_t},F_{y_t},F_{z_t},M_{x_t},M_{y_t},M_{z_t}\right]^T \tag{6}$$

### 3.3. Full fluid-structure coupling model

Note that the expressions of Eq.(1-6) have consistent accuracy. Two basic dynamic models are introduced for discussions, i.e.,

(1) Beam-Rotor aeroelastic model (BR-model) considers the natural vibration of the structure and the influence of $R_{aero}$.

(2) Wing-Rotor aeroelastic model (WR-model) considers the combined influence of the natural vibration of the structure, the wing aerodynamic force and $W_{aero}$.

Which are expressed by

$$\begin{aligned}
&-EI_y w^{(4)}-m_w\ddot{w}-m_w y_c\ddot{\theta}+L_w=0\\
&-EI_z v^{(4)}-m_w\ddot{v}=0\\
&GJ\theta''-m_w y_c\ddot{w}-m_w r^2\ddot{\theta}+M_w=0
\end{aligned} \tag{7}$$

$$\begin{aligned}
&EI_y w^{(3)}-m_t\left(\ddot{w}+y_t\ddot{\theta}\right)=F_{zt}\\
&EI_y w''+J_y\ddot{w}+m_t z_t\left(z_t\ddot{w}-y_t\ddot{v}\right)=-M_{yt}\\
&EI_z v^{(3)}-m_t\left(\ddot{v}-z_t\ddot{\theta}\right)=F_{yt}\\
&EI_z v''+J_z\ddot{v}+m_t y_t\left(y_t\ddot{v}-z_t\ddot{w}\right)+J_y\Omega\dot{\theta}=M_{zt}\\
&GJ\theta'+m_t z_t\left(\ddot{v}-z_t\ddot{\theta}\right)+m_t y_t\left(\ddot{w}+y_t\ddot{\theta}\right)+J_x\ddot{\theta}-J_y\Omega\dot{v}=M_{xt}
\end{aligned} \tag{8}$$

## 4. SOLUTIONS

The dynamic equation of the system is modeled by Rayleigh-Ritz method[6], and the deformation amount of each degree of freedom is approximately expressed as

$$\begin{bmatrix}w(x,t)\\v(x,t)\\\theta(x,t)\end{bmatrix}=\begin{bmatrix}\sum_{j=1}^{N_w}Q_{1j}\phi_{1j}^{trial}(x)\\\sum_{j=1}^{N_v}Q_{2j}\phi_{2j}^{trial}(x)\\\sum_{j=1}^{N_\theta}Q_{3j}\phi_{3j}^{trial}(x)\end{bmatrix}e^{i\xi t} \tag{9}$$

Wherein, $N_v$, $N_w$, and $N_\theta$ are the total orders of the $w$, $v$, and $\theta$ trial functions, respectively. $Q_{1j}$, $Q_{2j}$, and $Q_{3j}$ are coefficients of the trial function components of each order. $a$, $b$, and $c$ are the respective test functions. A set of high-accurate trial functions are introduced as following[6]

$$\begin{aligned}
\phi_1^{trial}&=\cosh(\gamma_w X)-\cos(\gamma_w X)\\
&+\frac{\sin(\gamma_w)-\sinh(\gamma_w)+M_t\gamma_w[\cos(\gamma_w)-\cosh(\gamma_w)]}{\cos(\gamma_w)+\cosh(\gamma_w)-M_t\gamma_w[\sin(\gamma_w)-\sinh(\gamma_w)]}[\sinh(\gamma_w X)-\cosh(\gamma_w X)]\\
\phi_2^{trial}&=\cosh(\gamma_v X)-\cos(\gamma_v X)\\
&+\frac{\sin(\gamma_v)-\sinh(\gamma_v)+M_t\gamma_v[\cos(\gamma_v)-\cosh(\gamma_v)]}{\cos(\gamma_v)+\cosh(\gamma_v)-M_t\gamma_v[\sin(\gamma_v)-\sinh(\gamma_v)]}[\sinh(\gamma_v X)-\cosh(\gamma_v X)]\\
\phi_3^{trial}&=\sin(\gamma_\theta)
\end{aligned} \tag{10}$$

After substituting Eq.(10) into the structural and aerodynamic equations of the system, the kinetic equation in vector manner is finally obtained:

BR-model

$$(p^2\mathbf{M}+p\boldsymbol{G}+K)\mathbf{Q}=0 \tag{11}$$

WR-model

$$(p^2\mathbf{M})\mathbf{Q}=\left[\frac{v_a{}^2k^2}{b^2}\mathbf{K}_f(k)-(\gamma+i\frac{v_a k}{b})\boldsymbol{G}-\boldsymbol{K}\right]\mathbf{Q} \tag{12}$$

Where $p$ is the complex root of the equation, $\gamma=real(p)$; $M$, $K_f$, $G$, $K$ are both $(N_v+N_w+N\theta)\times(N_v+N_w+N_\theta)$ order square matrix. $M$ contains the mass inertia characteristics of the system, $K_f$ contains the influence of the aerodynamic force of the wing, $G$ contains the influence of the structural gyro effect, and $K$ contains the elastic characteristics of the system. Herein, the improved p-k method is used for solution[9].



Presented at 46th European Rotorcraft Forum, Moscow, Russia, 8-11 September, 2020

## 5. CASE STUDIES

The reference data regarding actual configuration are introduced[6]. The distinct parameters about tilt angle and altitude are considered here for influence analyses.

### 5.1. Frequency analyses

Rotors usually gain greater lift and pitch control torque through tilt, wherein inertia change affects the structural characteristics and $R_{aero}$ also changes completely with $\alpha_p$. The tilt rotor changes the direction of angular momentum, which enhances the structural coupling. The airship experiences a flight span of *0-20 km* in VTOL task, and the air density also changes drastically, e.g., the air density in high-altitude flight is extremely thin. Structural and aerodynamic factors interact with each other, determining the modal characteristics of the system. Herein, baseline condition, $\alpha_p$*=45*◦ and *H=10 km* are included in the following analyses.

Fig. 5 illustrates the frequency properties of BR-model. The baseline result shows that R(a/b/c/f) are $R_{aero}$ aeroelastic modes and R(d/e) are close to structural modes. $\alpha_p$ has a significant impact on BR-model: except for BR(a/c), the frequency amplitude of each mode changes a little; BR(a) becomes [BD] at its initial stage, and BR(c) shows strong $R_{aero}$ aeroelastic coupling. The influence of altitude is also significant, the frequency amplitudes of BR (b/d/e/f) have small changes, and each mode is very close to natural frequency, BR(a) is in [F] state all along, and BR(c) is no longer divergent.

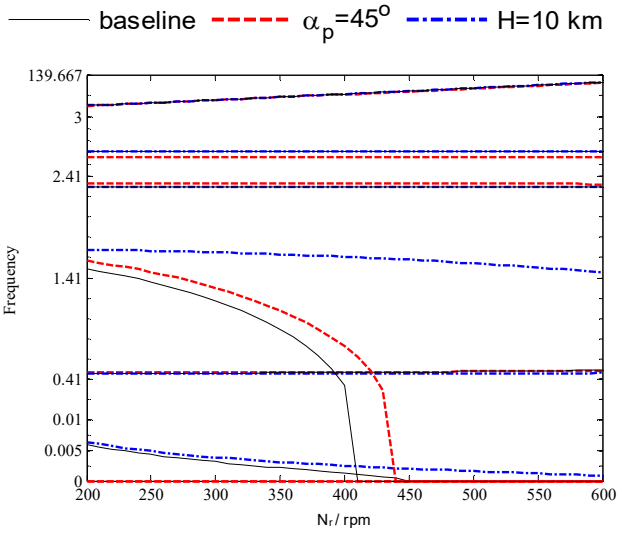


Fig. 5 The frequency spectrums of BR model (a~f denote 1st~6th frequency modes in order)

Fig. 6 shows the frequency properties of WR-model, where WR(a/b) are full aeroelastic coupling modes, WR(c/f) are $R_{aero}$ aeroelastic modes, and WR(d/e) are closer to the $W_{aero}$ aeroelastic modes. Under the variation of $\alpha_p$, the frequency amplitude of each mode changes a little, where WR(f) mode is hardly affected. Under the variation of *H*, WR(b/d/f) are almost unchanged, which are consistent with Fig. 5, and each mode are also very close to the natural frequency similarly.

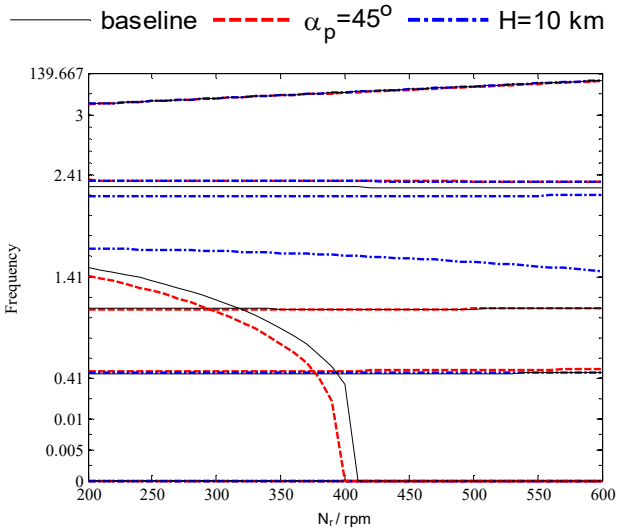


Fig. 6 The frequency spectrums of WR model (a~f denote 1st~6th frequency modes in order)

### 5.2. Parametric analyses

Fig. 7 reveals the influence law of $\alpha_p$. Both models are significantly affected, and the frequency curves show monotonous changes. When $N_r$*=0 rpm*: $\alpha_p$ has more significant effects on higher-order modes; the BR-model is in structural state; WR (a) is divergent; frequency crossing occurs between WR(b/c); the damping curves also show monotonous changes; WR(a/b) are hardly affected; the stability of WR(c/f) is increased, while the stability of WR(d/e) is reduced; the divergence phenomenon appears in WR(e). When $N_r$*=250 rpm*: with the increment of the gyro-effect and $R_{aero}$, the modal frequency has changed, e.g., WR/BR(c/f); the damping of BR/WR-models also changes severely; the damping in BR(b/d) become smaller, WR/BR(e) are in small damping modes, and WR/BR(c/f) are in relatively stable negative damping states. When $N_r$*=600 rpm*: the frequencies of WR/BR(c) become 0, while the frequencies of WR/BR(f) increase further; WR/BR(c) modes present [D]; the damping of WR/BR-model overall become stronger, e.g., WR/BR(a2/c/f). In general, the stability of WR/BR configuration decreases when tilt angle increases in high rotation speed.




Presented at 46th European Rotorcraft Forum, Moscow, Russia, 8-11 September, 2020

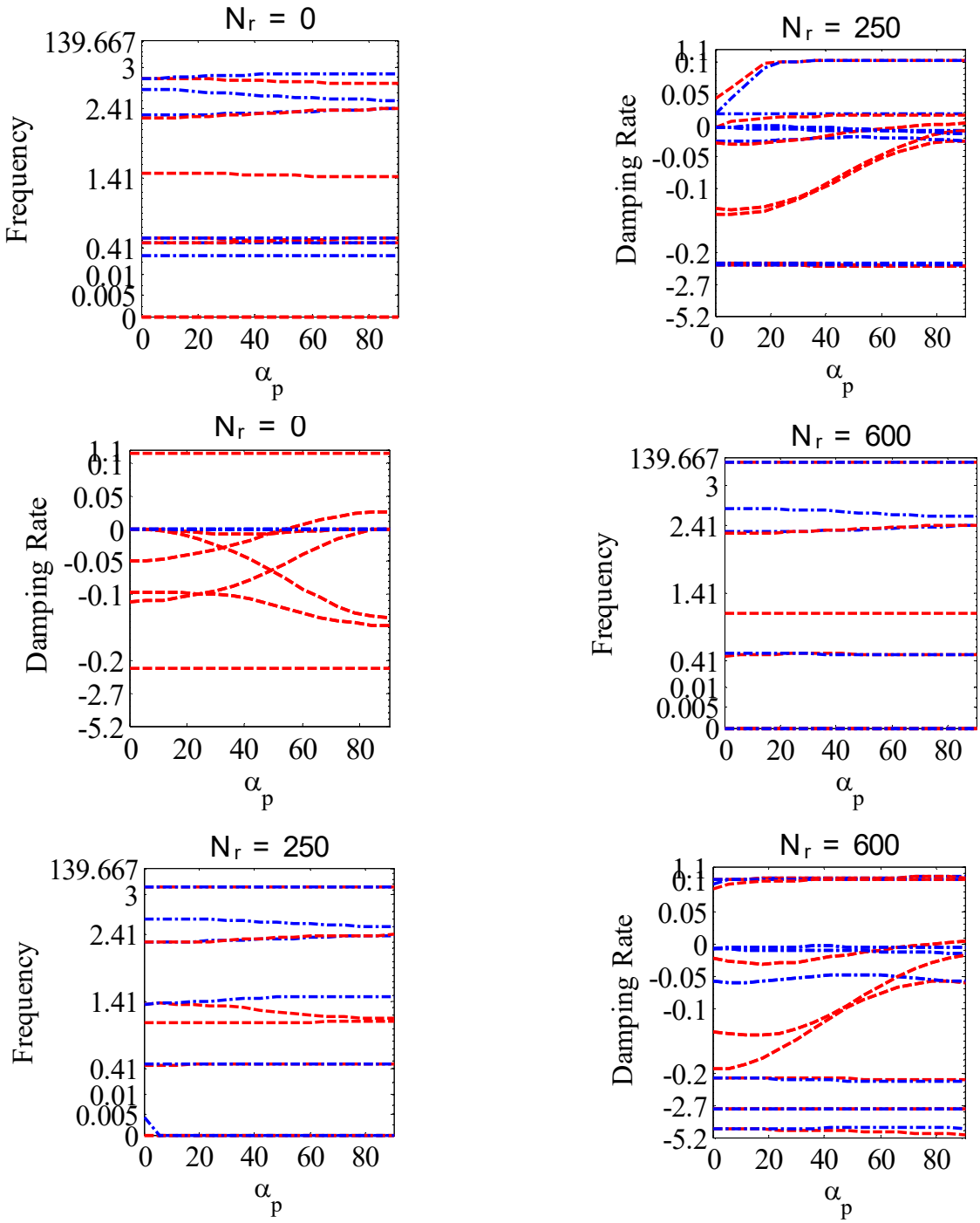


Fig. 7 Trends of modal properties with parameter $\alpha_p$ (a~f denote 1st~6th frequency modes in order)

Fig. 8 reveals the influence of the air condition. With the increase of *H*, the modal characteristics tend to converge toward the natural vibration state, and the curves of the two models approach to each other. When $N_r$*=0 rpm*: WR(a) is in [D] state at low altitude, because the $W_{aero}$ effect is weakened, the system changes from the real mode to the complex mode, and the damping bifurcation also disappears; When *H* is further increased, the difference between WR(a) and BR(a) reduce further; mode veering phenomenon occurs between WR(d/e), and the modal frequency curve changes accordingly; the damping is also present arched trends within the mode veering area. When $N_r$*=250 rpm*: The enhanced gyro-effect first redistributes the frequency amplitudes, e.g., (a/f) modes; frequency crossing appears between WR(c/e); WR(d/e) present mode veering phenomenon; due to the existence of $R_{aero}$, WR/BR-models still maintain certain order of aerodynamic damping; and the damping of each model decreases uniformly with the change of *H*, showing monotonic trends. When $N_r$*=600 rpm*: The gyro-effect further changes the frequency amplitudes, e.g., (a/f) modes; BR(a) and



Presented at 46th European Rotorcraft Forum, Moscow, Russia, 8-11 September, 2020

WR/BR(c) enter into [B] states by the enlarged $R_{aero}$; meanwhile, WR/BR(c) turn into complex mode states; the increment of speed makes the damping of WR/BR-models larger, e.g., WR/BR(a/c/f); the damping curves of each mode converge to the horizontal axis, and the change law is consistent with the frequency, e.g., WR/BR(c).

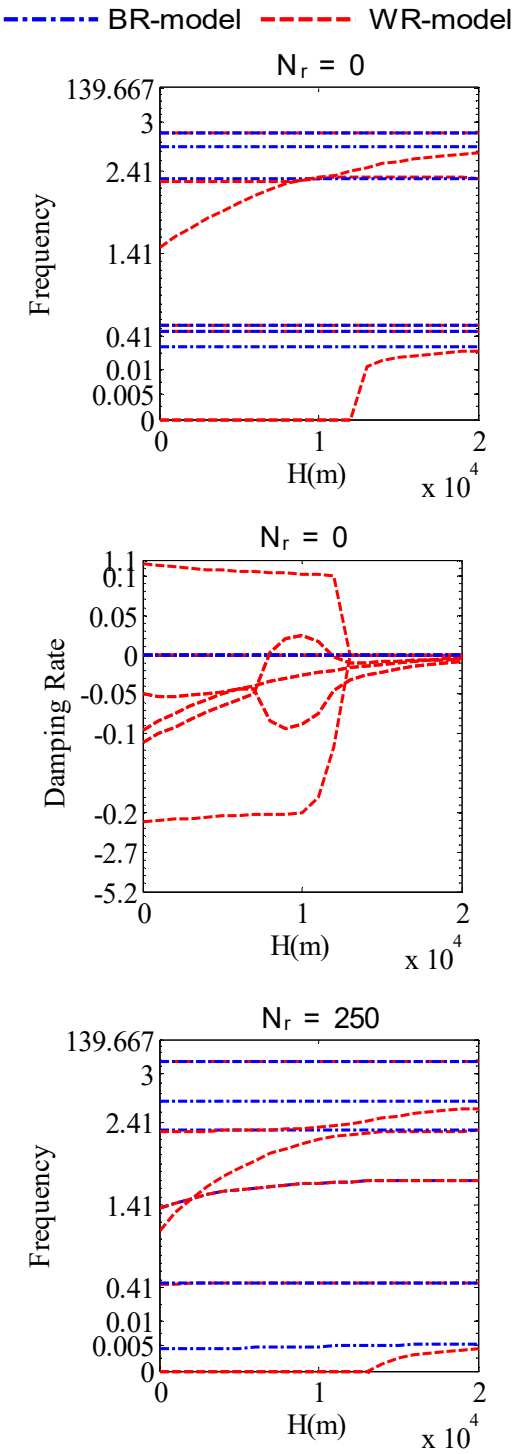


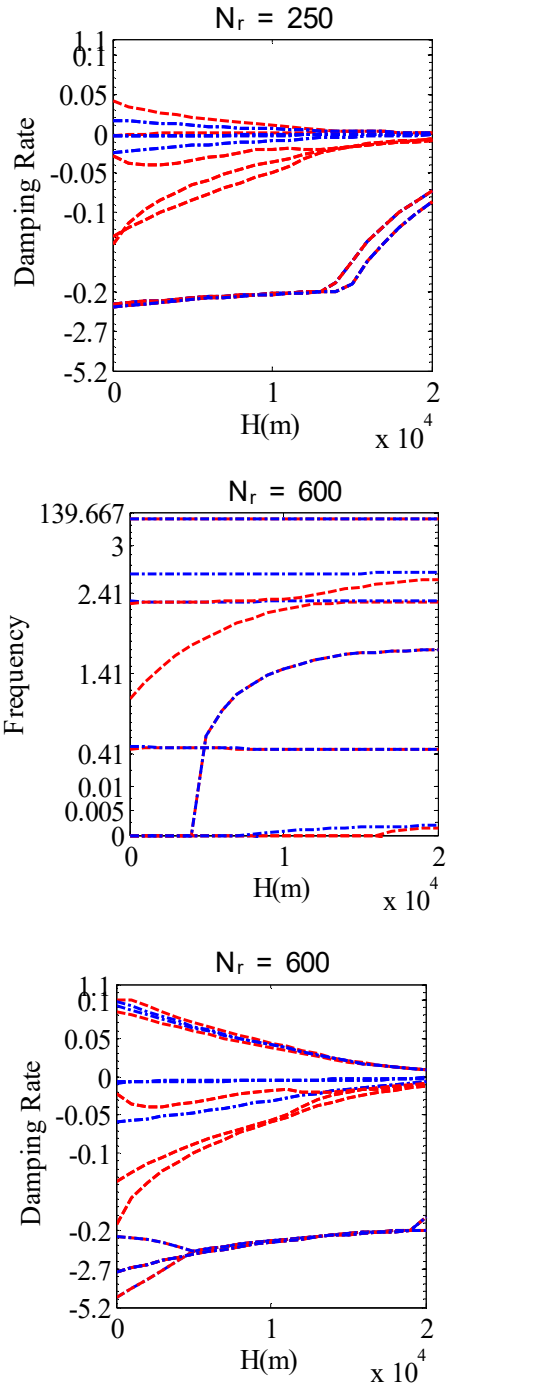


Fig. 8 Trends of modal properties with parameter *H* (a~f denote 1st~6th frequency modes in order)

Fig. 9 shows the effect of $K_W$ on the modal characteristics; the change of horizontal coordinate in the plots represents an increase of elastic axis stiffness in magnitude order. *Log($K_W$/baseline)=0* is equal to the exact baseline condition, and *log($K_w$/baseline)=4* indicates that the stiffness of elastic axis increases $10^4$ times compared with baseline condition. On the whole, the frequency curve increases exponentially with $K_W$, and the two models tend to approach each other to the



Presented at 46th European Rotorcraft Forum, Moscow, Russia, 8-11 September, 2020

superposition state at large stiffness; the damping performance shows that the system becomes more stable; the results of $N_r$=*250 rpm* and $N_r$=*600 rpm* show that the modal frequencies are more easily affected by $N_r$. In the case of $N_r$=*0 rpm*: the result of R-model is the natural property of the system, and its frequency curves present linear trends in the plots; the initial unstable WR-model changes from real mode to complex mode with the increase of $K_W$, which brings stable aerodynamic damping; the $W_{aero}$ coupling mode WR (e) also approaches to BR (e) with the change of $K_W$; when $K_W$>1, the damping of WR-model begins to change steadily; the R-model is affected by the change of stiffness, and the fluctuations of curves are obvious. In the case of $N_r$=*250 rpm*: the effect of $K_W$ is coupled with $N_r$, the frequency of the system changes obviously; the linear change trends of frequency curves change due to the gyro-effect, e.g., (f) mode. Mode veering phenomena appear between WR/BR (c) and WR/BR (f) modes; the results show that the increase of $K_W$ is beneficial to the stability of the system; when $K_W$>*1.7*, the damping of each mode is negative, and the bifurcation state of the system is also disappearing and entering the complex mode state; WR/BR (a) mode finally drops to the larger negative damping state; the damping of the system is improved by the increase of $K_W$. Under the influence of mode veering, the damping curves of WR/BR (c) and WR/BR (f) are separated obviously. In the case of $N_r$=*600 rpm*, the enhancement of gyro-effect firstly redistributes the frequency spectrum; compared with the $N_r$=*250 rpm* case, [B] phenomenon occurs in the initial stage of WR/BR (c); WR/BR (c) and WR/BR (f) still maintain apparent modal interactions. The results show that the variation of frequency is consistent with that of $N_r$=*250 rpm* case; the increase of $R_{aero}$ makes the damping amplitude of the system further increase, e.g., the BR (b/e/d) modes, and the stability of $K_W$ is delayed; all damping coefficients of the system become negative until $K_W$>*2.9*; under the strong influence of $R_{aero}$, the damping of WR-model also presents a similar change trend with BR-model. Generally speaking, $K_W$ is of great significance to the stability of the system. It is coupled with the influence of $N_r$ parameter, which makes the modal characteristics more complicated. The results show that large stiffness can change the instability of the system.

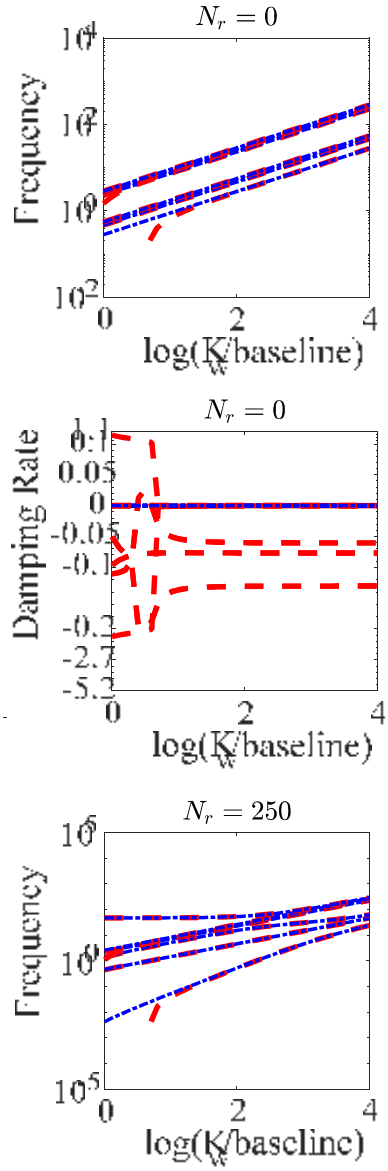


BR-model WR-model



Presented at 46th European Rotorcraft Forum, Moscow, Russia, 8-11 September, 2020

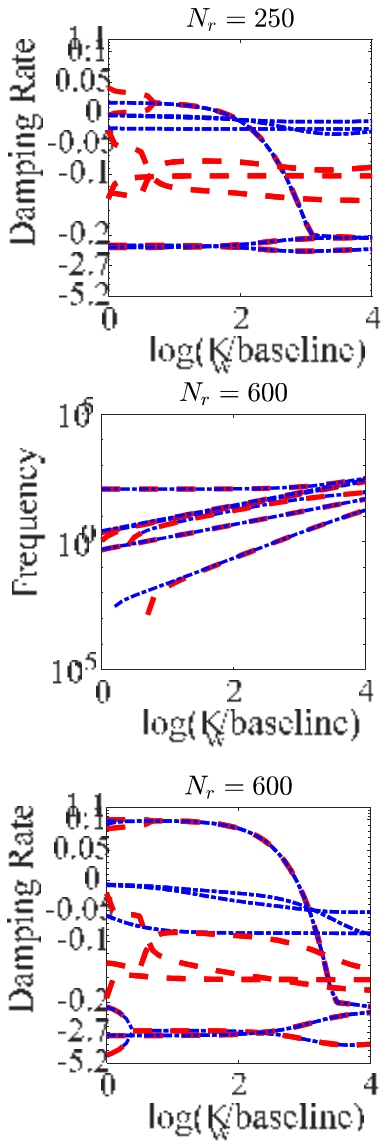


Fig. 9 Trends of modal properties with parameter $K_w$ (a~f denote 1st~6th frequency modes in order)

## 6. CONCLUSIONS

The physical models of the tilt-rotor system on airships are established by combining structural and aerodynamic modules. Two typical models are formed, i.e., BR-model and WR-model. The differential governing equations are solved by introducing Raleigh-Ritz numerical method. The aeroelastic performance of the system is evaluated through parametric studies, in which the most distinct and influential factors are considered. The results indicate that the rotation speed has significant influence on the modal frequency distributions, and in different air condition the system shows large changes in frequency performance. Mode veering phenomena are detected in certain circumstances, showing large implications on the modal damping. The combining effects of the inherent and external factors tend to complicate the entire aeroelastic performance of the system, which cannot be neglected in the initial preliminary structural design.

## ACKNOWLEDGEMENTS

This work is supported by the National Key Laboratory Foundation of China (no. 61422200101), the National Natural Science Foundation of China (nos. 11872211 and 11572156) and also the grants of NUAA (no. 90YAH19033).

## REFERENCES

[1] Collozza A., Dolce J. L. High-Altitude, Long-Endurance Airships for Coastal Surveillance[R]. Washington, DC: NASA, 2005.
[2] Azinheira J. R., Moutinho A., Paiva E. C. D. Airship Hover Stabilization Using a Backstepping Control Approach[J]. Journal of Guidance Control and Dynamics, 2006, 29(4):903–914.
[3] Jianguo G., Jun Z.. Review of the Control of Low Dynamic Vehicles in Near Space[J]. Acta Aeronautica et Astronautica Sinica, 2014, 35(2):320–331.
[4] Jeffrey L., Singe P. W. China Tests Its Largest Airship[J]. Popular Science, 2015:89–95.
[5] Xiayang Z., Haoquan L., Xiao G., et al. Several Concerns of Advanced Airships for Thrust-Vectoring Application on Dynamic Study[C]. AIAA Lighter-Than-Air Systems Technology Conference, Denver, Colorado: AIAA, 2017.
[6] Xiayang Z., Ming Z., Meijuan Z., et al. Frequency Analysis of Wing–Rotor System Considering Flexibility in Capsule Based on High-Accurate Method[J], International Journal of Aeronautical and Space Sciences, 2018, 19(2): 375-387.
[7] Xiayang Z., Meijuan Z., Haoquan L., et al. Structural and Aeroelastic Analyses of a Wing with Tip Rotor[J]. Journal of Fluids and Structures, 2019, 86:44-69.
[8] Yeo H., Johnson W. Performance and Design Investigation of Heavy Lift Tilt-Rotor with Aerodynamic Interference Effects[J]. Journal of Aircraft, 2009, 46(4):1231–1239.
[9] Gu Y, Yang Z. Modified p-k Method for Flutter Solution with Damping Iteration[J]. AIAA Journal, 2015, 50(2):507-510.



Presented at 46th European Rotorcraft Forum, Moscow, Russia, 8-11 September, 2020